An Integrated Experimental and Computational Approach for Characterizing the Kinetics and Mechanism of Triadimefon Racemization

QIANYI CHENG,[1] QUINCY TENG,[2] SATORI A. MARCHITTI,[3] CALEB M. DILLINGHAM[1] AND JOHN F. KENNEKE[2]*

[1]*Student Services Authority Contractor, National Exposure Research Laboratory, U.S. Environmental Protection Agency, Athens, Georgia, USA*
[2]*National Exposure Research Laboratory, U.S. Environmental Protection Agency, Athens, Georgia, USA*
[3]*ORISE Fellow, National Exposure Research Laboratory, U.S. Environmental Protection Agency, Athens, Georgia, USA*

ABSTRACT Enantiomers of chiral molecules commonly exhibit differing pharmacokinetics and toxicities, which can introduce significant uncertainty when evaluating biological and environmental fates and potential risks to humans and the environment. However, racemization (the irreversible transformation of one enantiomer into the racemic mixture) and enantiomerization (the reversible conversion of one enantiomer into the other) are poorly understood. To better understand these processes, we investigated the chiral fungicide, triadimefon, which undergoes racemization in soils, water, and organic solvents. Nuclear magnetic resonance (NMR) and gas chromatography / mass spectrometry (GC/MS) techniques were used to measure the rates of enantiomerization and racemization, deuterium isotope effects, and activation energies for triadimefon in H_2O and D_2O. From these results we were able to determine that: 1) the alpha-carbonyl carbon of triadimefon is the reaction site; 2) cleavage of the C-H (C-D) bond is the rate-determining step; 3) the reaction is base-catalyzed; and 4) the reaction likely involves a symmetrical intermediate. The B3LYP/6–311 + G** level of theory was used to compute optimized geometries, harmonic vibrational frequencies, nature population analysis, and intrinsic reaction coordinates for triadimefon in water and three racemization pathways were hypothesized. This work provides an initial step in developing predictive, structure-based models that are needed to identify compounds of concern that may undergo racemization. *Chirality 00:000–000, 2016.*

KEY WORDS: chirality; conazoles; enantiomerization; environmental chemicals; pesticides; risk assessment; stereochemistry

Chiral molecules possess at least two nonsuperimposable mirror images (enantiomers) and may have additional stereoisomers depending on the number of asymmetric centers. As a result of this "mixture" a chiral molecule in a chiral environment (e.g., biological system containing enzymes) will typically exhibit more varied and complex interactions than an achiral molecule. This is illustrated by the fact that enantiomers commonly exhibit different environmental fates, pharmacokinetics, and toxicities. Ignoring these differences can introduce significant uncertainty in understanding and modeling the physiological and environmental fate of chiral chemicals and evaluating their risk to human health and the environment. While it is common practice to evaluate the impact of chirality on the efficacy and safety of pharmaceuticals, this is typically not the case for chemicals of environmental concern (e.g., pesticides). There is an even greater dearth of stereoisomer-specific information regarding unintentional exposures (outside the scope of product use) such as chiral pharmaceuticals released into the environment[1] and humans exposed to chiral pesticides.[2]

Approximately half of all pharmaceuticals are chiral compounds, with a significant number produced as pure enantiomers.[3] More than 30% of pesticides are chiral; however, in most cases the racemic material is used even though the pesticidal activity typically resides in one enantiomer (or several stereoisomers when there is more than one chiral center). In an effort to reduce the unnecessary environmental burden of inactive stereoisomers, there has been a movement to implement a "chiral switch" where the racemic mixture is replaced with the most active stereoisomer(s). To that end, the U.S. Environmental Protection Agency (U.S. EPA) has issued an interim policy for stereoisomeric pesticides to determine whether the enriched mixture(s) are of greater concern environmentally and from a human health perspective than the racemic mixture.[4] The European Union has revised regulations so that plant protection products containing significant proportions of inactive stereoisomers become a candidate for chiral switch.[5]

The scientific literature contains many reports on the stereoselective transformation of chiral compounds under biological and environmental conditions; in many cases one enantiomer is preferentially degraded or metabolized. Far less information, however, exists on the biological and environmental racemization (and enantiomerization) of chiral compounds. Racemization is the macroscopic statistical process of the irreversible transformation of one enantiomer into the racemic mixture, while enantiomerization refers to the microscopic and molecular process of the reversible conversion of one enantiomer into the other.[6] Racemization has been found

*Correspondence to: J. F. Kenneke, U.S. Environmental Protection Agency, 960 College Station Road, Athens, Georgia 30605. E-mail: kenneke.john@epa.gov
Received for publication 19 May 2016; Accepted 24 June 2016
DOI: 10.1002/chir.22622
Published online in Wiley Online Library (wileyonlinelibrary.com).

to occur with pharmaceuticals[7] and pesticides[8] and is a point of emerging concern. Due to differences in stereospecific toxicity and efficacy, it is critical to assess the potential for a compound to undergo racemization. In terms of use and application, if racemization occurs quickly it would not make sense to use a chiral switch or develop enantiopure pharmaceuticals and pesticides. Racemization can also have a profound impact on sample preparation, storage, and analysis—especially if it occurs unknowingly. For these reasons, when evaluating the exposure and effects of chiral compounds it is imperative to consider configurational instability under environmental and biological conditions.

Recent studies have shown that some chiral, 1,2,4-triazole fungicides can undergo racemization.[8] Triazole fungicides have both medical and agricultural applications and some of these have been detected in surface and waste waters[9] and in human and ecological biomonitoring studies.[10] Triadimefon [(RS)-1-(4-chlorophenoxy)-3,3-dimethyl-1-(1H-1,2,4-triazol-1-yl)butan-2-one] (Fig. 1) is a chiral systemic broad-spectrum 1,2,4-triazole fungicide that is used on ornamentals and food crops. It has been shown that R-triadimefon is 2-fold more toxic than the racemate to blackfly larvae[11] and under biological conditions, the prochiral carbonyl of both R- and S-triadimefon undergoes stereoselective reduction[12] to yield four stereoisomers of triadimenol.[13] As with triadimefon, triadimenol is a registered fungicide and studies have shown that the 1S,2R-triadimenol stereoisomer (produced from S-triadimefon) exhibits 1000-fold greater fungicidal activity[14] and greater inhibition of sterol synthesis than the other stereoisomers.[15] A potential complicating factor in assessing the risk of triadimefon and triadimenol is the fact that triadimefon has been shown to undergo varying degrees of racemization in soils, water, and organic solvents.[12,13,16,17] Thus, the degree of racemization could impact the distribution of triadimenol stereoisomers that are formed from the metabolism or environmental transformation of triadimefon.

A variety of mechanisms have been proposed to account for the racemization of chiral compounds including: keto-enol tautomerization, resonance-stabilized carbanion intermediates, and base catalysis involving a transition state with the proton halfway between the base and the chiral carbon.[18] In the case of triadimefon, several crystallographic studies[8,19–21] and laboratory studies[8] have been conducted and racemization was hypothesized to be related to the acidity of the α-hydrogen; however, detailed kinetic studies examining microscopic and macroscopic rate constants were not conducted nor was a mechanism of racemization developed.

Here we combine experimental and computational studies for the first time to characterize the kinetics and mechanism for the racemization of triadimefon under physiological and environmentally relevant conditions. By delineating the kinetics and mechanism of racemization, this work provides an initial step in developing predictive, structure-based models that are needed to identify quickly both pharmaceutical and nonpharmaceutical compounds that may undergo racemization. Such models will not only aid in evaluating chemicals for chiral switch and enantiopure applications, but also provide a means for improving human health and ecological risk assessment by identifying chemicals that may require specialized testing.

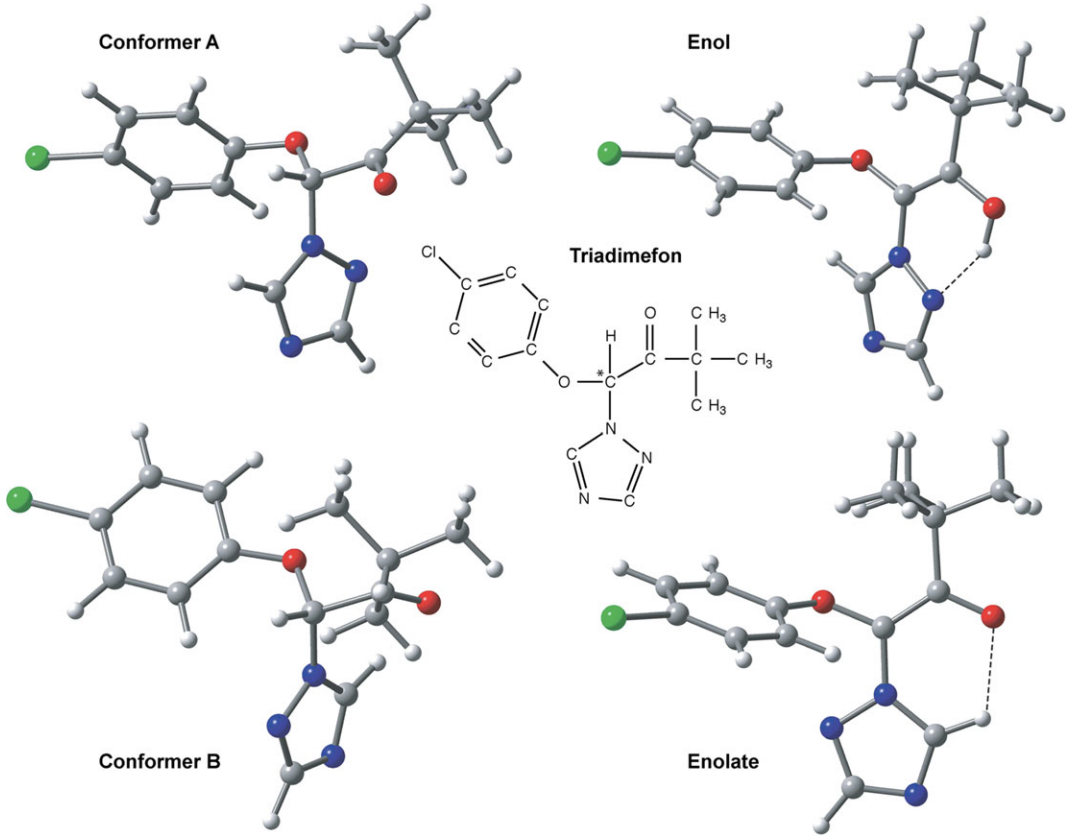

Fig. 1. Structures of two low-energy R-triadimefon conformers (A and B), and their possible enol and enolate products. The chiral center is marked with *

MATERIALS AND METHODS

Chemicals

Triadimefon [(RS)-1-(4-chlorophenoxy)-3,3-dimethyl-1-(1H-1,2,4-triazol-1-yl)butan-2-one] (99.4% purity) was obtained from the U.S. EPA National Pesticide Standard Repository (Ft. Meade, MD) and was separated (Chiral Technologies, West Chester, PA) into its two enantiomers using preparative supercritical fluid chromatography as previously described.[13] All other chemicals were obtained from Sigma-Aldrich (St. Louis, MO) and were reagent grade or better.

H/D Substitution Rates

S and R triadimefon (2 mg) was added to 0.5 mL 100% D_2O with 20 μM 2,2-dimethyl-2-silapentane-5-sulfonate sodium salt (DSS; added as a matrix internal standard) in a 2-mL microcentrifuge tube containing a 3.2-mm stainless-steel bead. The tube was shaken using a tissuelyser (Qiagen, Valencia, CA) at 20 Hz for 3 min. Subsequently, the sample was centrifuged at 10,000 *g* for 2 min and 230 μL of the sample was transferred into a 3-mm nuclear magnetic resonance (NMR) tube for NMR analysis.

All NMR spectra were acquired on an Agilent (Palo Alto, CA) Inova 600 MHz NMR spectrometer using a 3-mm triple-resonance probe. A series of presaturation spectra measured at 25°C, 35°C, 45°C, and 55°C were collected with 2-sec presaturation time, 2-sec acquisition time and 288 transients (or scans), with the exception that the spectra measured at 35°C were collected with 96 transients. Peak identities were assigned based on Carbonell's result.[22] The integrated signal at 7.30 ppm corresponding to the α-hydrogen located on the chiral carbon of triadimefon was monitored to evaluate the rate of H/D exchange (deuteration). The concentration of triadimefon in each sample was calculated using the peak area at 7.30 ppm relative to the DSS peak at 0.0 ppm. Least-squares linear regression of the natural logarithm of the signal normalized to the DSS peak area as a function of time was used to calculate pseudo-first-order rate constants of H/D substitution (k_{deut}) for each experimental temperature.[18]

Racemization Rates

A set of 7–10 samples containing 500 μL of pH buffer (pH 1 to pH 9) were placed in a thermostatically controlled heating block. After 10 min, 5 μL of concentrated triadimefon enantiomer stock (in acetonitrile) was added to each sample and vortexed to yield a final enantiomer concentration of 35 μM. At selected times, 500 μL of methyl-t-butyl ether (MTBE) was added to individual sample tubes and vortexed; the MTBE layer was then removed and transferred to a gas chromatography (GC) vial containing a micro-insert. MTBE extracts were analyzed by gas chromatography mass spectrometry (GC/MS) (Hewlett-Packard 6890/5973) equipped with a BGB 172 chiral capillary column (BGB Analytik, Switzerland) as previously described.[13] Enantiomers of triadimefon were detected and quantified using selected ion monitoring (SIM) at m/z 181, 208, and 210. The triadimefon enantiomeric excess (ee) was calculated as:

$$ee = \frac{[TFN_a]_t - [TFN_b]_t}{[TFN_a]_t + [TFN_b]_t} \quad (1)$$

where $[TFN_a]_t$ is the concentration of one of the triadimefon enantiomers and $[TFN_b]_t$ is the concentration of the other triadimefon enantiomer at time t. Least-squares linear regression was applied to the natural logarithm of *ee* as a function of t to calculate pseudo-first-order rate constants of racemization (k_{rac}) for each experimental pH.[18] Additional studies were conducted with 100 mM phosphate buffer prepared with either H_2O (pH 7.4) or 99 + % D_2O (pD 7.8) and were maintained at four selected temperatures ranging from 25°C to 55°C. Mass spectra were collected in SIM mode as described above, including m/z 182, 209, and 211. Pseudo-first-order rate constants of racemization in H_2O (k_{racH}) and D_2O (k_{racD}) were calculated using eq. 1 as described for k_{rac}.

Thermodynamic Properties

Activation energies (E_a) were calculated for the racemization reaction according to the Arrhenius equation:

$$k = Ae^{-E_a/RT} \quad (2)$$

Rearranging (2) yields:

$$\ln(k) = -\frac{E_a}{R}\left(\frac{1}{T}\right) + \ln(A) \quad (3)$$

RT where k is the rate constant of racemization (k_{racH} and k_{racD}), A is the pre-exponential factor, R (1.9872 × 10^{-3} kcal mol^{-1} K^{-1}) is the universal gas constant, and T is the absolute temperature. Least-squares linear regression was applied to Arrhenius plots of $\ln(k_{racH})$ and $\ln(k_{racD})$ as a function of 1/T yielding a slope of $-E_a/R$. The Gibbs energy of activation $\Delta G^{\ddagger}$ was calculated according to the Eyring equation:

$$\Delta G^{\ddagger} = -RT\ln\left(\frac{k_i h}{k_B T}\right) \quad (4)$$

where k_i is the measured reaction rate constant k_{deut}, k_{racH}, and k_{racD}, T is the absolute temperature, h (6.6261 × 10^{-34} m^2 kg s^{-1}) is Planck's constant, and k_B (1.3806 × 10^{-23} m^2 kg s^{-2} K^{-1}) is the Boltzmann constant.

Theoretical Methods

We applied one of the most commonly used hybrid functionals of density functional theory (DFT), the B3LYP functional,[23–25] with 6–311 + G** basis set which is helpful for anion-involved computations. B3LYP/6–311 + G** has consistently provided good results for organic molecules.[26,27] Optimized geometries, harmonic vibrational frequencies, nature population analysis,[28–31] and intrinsic reaction coordinates (IRC) [32–35] were computed with the GAUSSIAN 09 package, which generates approximate numerical solutions of the governing quantum-model equation.[36]

RESULTS AND DISCUSSION

EXPERIMENTAL: Site of Deuterium Exchange

Full-scan mass spectra of MTBE extracts from studies conducted with triadimefon and D_2O exhibited an increase of 1 m/z for molecular fragments containing the α-carbonyl carbon of triadimefon. ^{1}H-NMR studies conducted with triadimefon and D_2O exhibited a continual decrease in the singlet at 7.30 ppm indicating deuterium exchange with the labile α-hydrogen of triadimefon. Both studies confirm that the α-carbonyl carbon of triadimefon is the site of reaction.

H/D Exchange and Racemization

The activation energies (E_a) measured for racemization of R-and S-triadimefon were 21.2 and 22.6 kcal mol^{-1} in D_2O and 21.4 and 21.4 kcal mol^{-1} in H_2O (Table 1). The similarity of these values suggests that R- and S-triadimefon have the same mechanism of racemization.

Since racemization and deuteration can proceed at different rates, it is critical to measure racemization (chiral GC/MS) and H/D exchange (^{1}H-NMR) separately. As shown in Table 1, the ratio of k_{deut} to k_{racD} for S- and R-triadimefon range from 0.71 to 0.93 and suggests that deuteration occurs with complete racemization and that both deuteration and racemization share a common mechanism. These results further suggest that the reaction mechanism involves a symmetrical intermediate such as a neutral enol, carbanion, or enolate (carbanion resonance structure).[37]

pH Effects

Studies conducted between pH 1 and pH 5 did not exhibit any appreciable racemization over a 24-h period. For studies conducted from pH 6 to pH 9 (Table 1), the rate of racemization (k_{racH}) increased linearly with increasing pH for both R- and S-triadimefon (r^2 = 0.995 and 0.996) and supports a general base-catalyzed mechanism of racemization. In base-

TABLE 1. Rate constants for deuteration (k_{deut}, × 10^{-3} min^{-1}), rate constant for racemization [in D_2O (k_{racD}, × 10^{-3} min^{-1}) and H_2O (k_{racH}, × 10^{-3} min^{-1})], with the corresponding Gibbs energies of activation ($\Delta G^{\ddagger}$, in kcal mol^{-1}) of triadimefon enantiomers at different reaction temperatures (in °C) and pH (pD)

Temp	pH or pD	k_{deut}	k_{racD}	k_{racH}	k_{deut}/k_{racD}	k_{deut}/k_{racH}	$\Delta G^{\ddagger}(k_{deut})$	$\Delta G^{\ddagger}(k_{racD})$	$\Delta G^{\ddagger}(k_{racH})$
S-Triadimefon									
25	6.0	—	—	0.1	—	—	—	—	25.4
25	7.0	—	—	1.0	—	—	—	—	24.0
25	7.8	1.7	1.8	5.0[a]	0.93	2.7	23.7	23.7	23.1
35	7.8	6.0	6.5	14.7[a]	0.91	2.2	23.8	23.7	23.2
45	7.8	—	19.8	45.4[a]	—	2.3	—	23.8	23.3
55	7.8	—	59.8	135.3[a]	—	2.3	—	23.8	23.3
25	8.0	—	—	7.4	—	—	—	—	22.8
25	9.0	—	—	64.0	—	—	—	—	21.6
E_a	—	—	22.6	21.4	—	—	—	—	—
R-Triadimefon									
25	6.0	—	—	0.1	—	—	—	—	25.4
25	7.0	—	—	1.3	—	—	—	—	23.9
25	7.8	1. 9	2.7	8.1[a]	0.71	3.0	23.8	23.4	22.8
35	7.8	—	9.0	33.2[a]	—	3.7	—	23.5	22.7
45	7.8	—	30.1	78.6[a]	—	2.6	—	23.5	22.9
55	7.8	—	68.8	239.4[a]	—	3.5	—	23.7	23.4
25	8.0	—	—	11.0	—	—	—	—	22.6
25	9.0	—	—	138.5	—	—	—	—	21.1
E_a	—	—	21.2	21.4	—	—	—	—	—

Measured at pH 7.4 and corrected to pH 7.8 using univariate linear model developed from $\ln(k_{racH})$ as a function of pH and Arrhenius plot described in text.

catalyzed racemization, proton abstraction to form a carbanion is likely the rate determining step.[38]

Isotope Effects

Comparing the rates of triadimefon racemization in H_2O and D_2O under various conditions (k_{racH} /k_{racD}; Table 1) reveals a significant isotope effect ranging from 2.2 to 3.7 and is within the range of isotope effects that have been reported for the α-hydrogen of ketones.[38,39] These results suggest that cleavage of the C-H (C-D) bond is the rate-determining step for the racemization of triadimefon in water.

Computational: R-Triadimefon Conformers

For chiral molecules, enantiomers possess identical physical and chemical properties as illustrated by the similar values of E_a we measured for R- and S-triadimefon in H_2O and D_2O (Table 1). Thus, our computational approach for R-triadimefon is also applicable to S-triadimefon.

Two low-energy conformations (A and B) of R-triadimefon (Fig. 1) were computed in this study, and the optimized geometries for the two conformers are shown in Supporting Table S1.

In conformer B there are two hydrogen bonds near the chiral center ($H_1 \cdots N_2$ = 2.42 Å and $H_8 \cdots O_2$ = 2.68 Å), while there is only one hydrogen bond ($H_1 \cdots O_2$ = 2.51 Å) in A. This difference may explain why B is approximately 3 kcal mol^{-1} lower in energy than A (Fig. 1).

Racemization Mechanism

Based on our experimental observations (the α-carbonyl carbon of triadimefon is the site of reaction), cleavage of the C-H (C-D) bond is the rate-determining step, the reaction is base-catalyzed, and the reaction likely involves a symmetrical intermediate along with our computed geometries, as well as the charge distributions for conformer A and B (Fig. S2), we hypothesize three racemization pathways: conformer A reaction with one water molecule, conformer A reaction with two water molecules, and conformer B reaction with hydroxide ion.

Conformer A Reaction With One Water

The reaction pathway of R-triadimefon conformer A with one water molecule is shown in Figure 2, where H_1 is abstracted by water, then replaced by a hydrogen atom from water. The optimized geometries of the six reactant complexes, transition states, and product complexes for the one water reaction pathway are listed in Table S2.

Initially, water binds to conformer A, forming a six-membered ring with two hydrogen bonds in reactant complex 1 (**RC1**$_{1w}$: $O_a \cdots H_1$ and $H_b \cdots O_2$ with lengths 2.38 Å and 1.99 Å), respectively. One O−H bond of water is slightly longer than the other (0.97 and 0.96 Å) since the longer one is involved in hydrogen bonding with conformer A. There are no large bond length changes in the rest of conformer A. $\tau_{H1C1N1C8}$ changes from 6.3° to 3.1° (in the free rotation range). In the transition state (**TS1**$_{1w}$), as the reaction proceeds, the C_2-O_2 bond length changes significantly from 1.21 Å to 1.27 Å, and the H_b from water migrates much closer to O_2 (1.17 Å) and away from O_a (1.27 Å). Meanwhile, H_1-O_a shortens to 1.18 Å, C_1-H_1 elongates to 1.49 Å in the six-membered ring. The H_1 is not only pulled away from C_1, but also out of the triazole plane, resulting in $\tau H_1C_1N_1C_8$ 34.4°. In product complex 1(**PC1**$_{1w}$), C_2-O_2 elongates to 1.35 Å, which is more like a single bond. H_b bonds to the O_2 in an enol form while C_1-C_2 shortens to a length in the double bond range (1.35 Å). H_1 is abstracted from C_1 and the distance between the two is over 4.0 Å. H_1-O_a now has normal water bond length of 0.97 Å, and H_1 bonds to N_4 (2.39 Å) forming a long hydrogen bond, which lowers the energy of **PC1**$_{1w}$. The newly formed water ($H_1O_aH_c$) easily breaks from the product complex leaving the enol (Fig. 1). H_b-O_2-C_2-C_1 and the triazole ring are co-planer forming a new ring with one hydrogen bond ($H_b \cdots N_2$ = 1.77 Å).

After the enol forms in the solution, a water molecule attacks the enol product from the right side of the triazole ring in reactant complex 2 (**RC2**$_{1w}$). The $H_e \cdots C_1$ is 4.16 Å, O_d-H_f

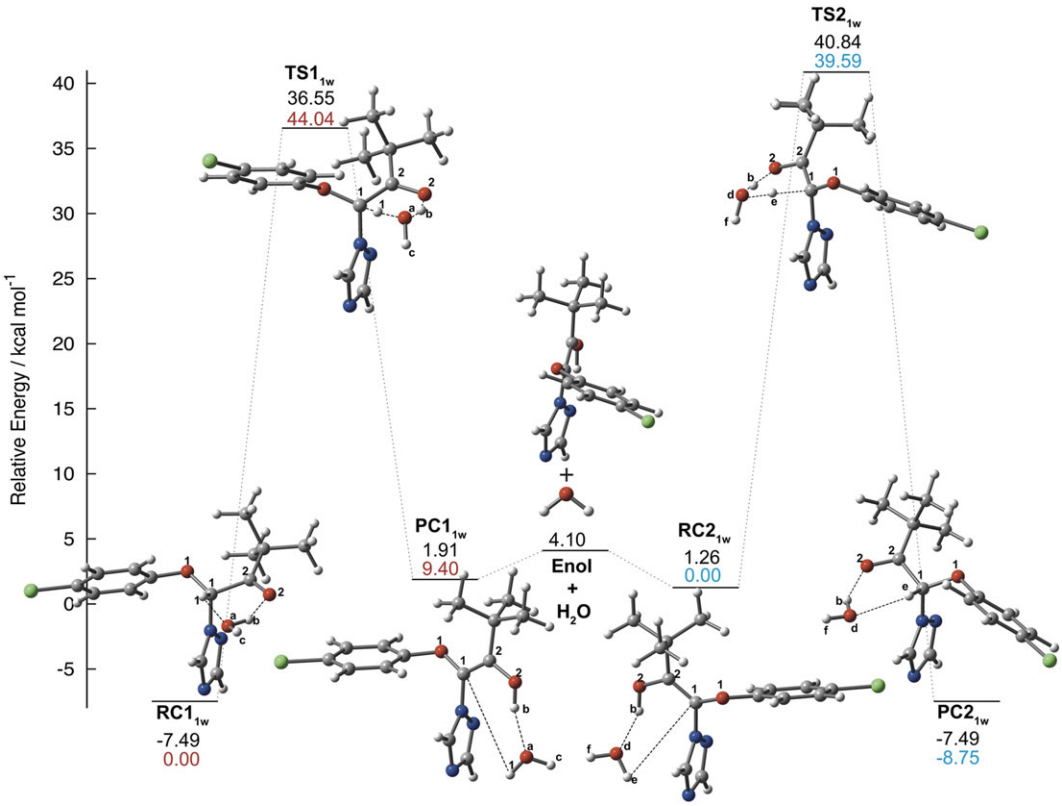

Fig. 2. Potential energy surface for the reaction of R-triadimefon conformer A with one water molecule. Energies in black are relative energies compared to the separated reactants: conformer A and water molecule; energies in red are relative energies compared to reactant complex **RC1**$_{1W}$; and energies in blue are relative energies compared to reactant complex **RC2**$_{1W}$. All energies are in kcal mol^{-1}

is 0.96 Å slightly shorter than O_2-H_b (0.98 Å), and now C_2-O_2 elongates to 1.35 Å. As the reaction proceeds, the water molecule, six-membered ring, and the t-butyl group rotate along the C_1-N_1 bond. The water moves to the left side of the triazole ring in the transition state 2 (**TS2**$_{1w}$), forming a new six-membered ring (C_2-O_2-H_b-O_d-H_e-C_1) with bond length changes: 1.35 to 1.28 Å in C_2-O_2, 0.98 to 1.28 Å in O_2-H_b, 1.90 to 1.16 Å in H_b-O_d, 0.97 to 1.18 Å in O_d-H_e, 4.16 to 1.52 Å in H_e-C_1, and 1.35 to 1.45 Å in C_1-C_2. C-C is more like a single bond in **TS2**$_{1w}$, while C-O is more like a double bond. In the product complex 2 (**PC2**$_{1w}$), C_1-C_2 elongates to 1.56 Å while C_2-O_2 continuously shortens to 1.21 Å. H_b bonds much more tightly to O_d forming a normal water bond (0.97 Å) while the O_2-H_b length elongates to 1.99 Å. H_e transfers to C_1 (1.09 Å) in **PC2**$_{1w}$, forming a $H_2O\cdots$S-triadimefon complex.

For this reaction pathway (Fig. 2), it is favorable for **RC1**$_{1w}$ to form, since it is −7.49 kcal mol^{-1} lower in energy than the separated conformer A plus one water molecule. However, the 36.55 kcal mol^{-1} activation barrier is much higher than our experimentally calculated results (Table 1), and the local barrier is even higher (44.0 kcal mol^{-1}).

PC1$_{1w}$ is higher in energy compared to the separated reactants, but by only 1.9 kcal mol^{-1}. An enol is formed after the water leaves **PC1**$_{1w}$, which lies 4.1 kcal mol^{-1} above conformer A. **RC2**$_{1w}$ is 1.26 kcal mol^{-1} lower in energy than the separated conformer A and water reactants, and 2.84 kcal mol-1 lower than the separated enol + water, which leads to a high local barrier (40.63 kcal mol^{-1}) and activation barrier (40.84 kcal mol^{-1}). **PC2**$_{1w}$ lies 7.49 kcal mol^{-1} below conformer A + H_2O, 11.59 kcal mol^{-1} below enol + H_2O, and 8.75 below **RC2**$_{1w}$, driving the reaction to form the final product complex.

The reaction enthalpy, entropy, and Gibbs energy for reaction **RC1**$_{1w}$ → **TS1**$_{1w}$ → **PC1**$_{1w}$ are shown in Table S3, which indicate that this part of the reaction is endothermic and would not occur spontaneously. However, after the enol is formed, the reaction **RC2**$_{1w}$ → **PC2**$_{1w}$, which leads to the formation of S-triadimefon, is exothermic and spontaneous. These computational results help explain why the enol could not be easily captured and lead to the formation of the other enantiomer.

Conformer A Reaction With Two Water Molecules

Because both the activation and local barriers for the one water racemization pathway are high, a reaction pathway involving two water molecules was also examined in this study (Fig. 3). The local barriers for transition state 1 (**TS1**$_{2w}$, 40.99 kcal mol^{-1}, Table S4) and transition state 2 (**TS2**$_{2w}$, 35.59 kcal mol^{-1}) are 3.05 kcal mol^{-1} and 4.00 kcal mol^{-1} lower respectively, and more favorable than for the one water pathway. The activation barriers are reduced to 23.11 kcal mol^{-1} for **TS1**$_{2w}$, and 24.80 kcal mol^{-1} for **TS2**$_{2w}$, which are much lower than those in our one water pathway (36.55 and 40.84 kcal mol^{-1}, respectively), and in much better agreement with the experiment calculated E_a (21.7 kcal mol^{-1}, average of R- and S-triadimefon racemization). When two water molecules bond to the chiral center an eight-membered ring in the reactant complex 1 (**RC1**$_{2w}$) is formed, where the ring strain may be reduced more than that in the six-membered ring of **RC1**$_{1w}$. Thus, the total energy of **RC1**$_{2w}$ is 17.88 kcal mol^{-1} well below the separated conformer A and two water molecules. After passing over **TS1**$_{2w}$, the

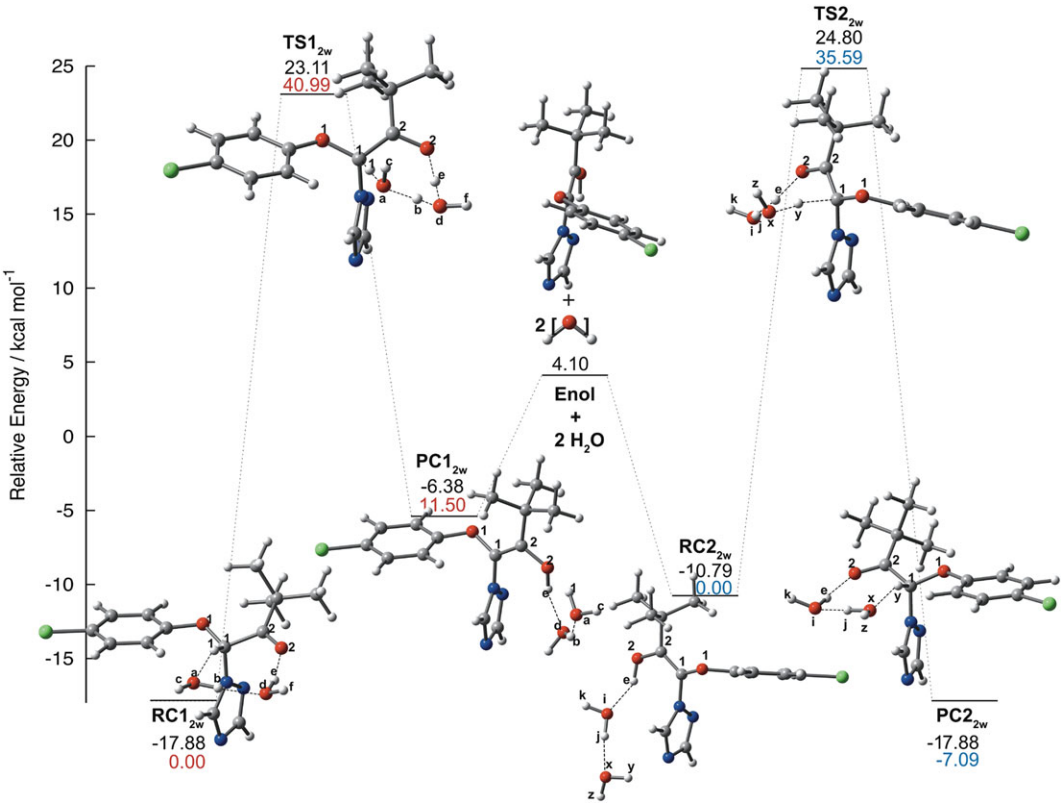

Fig. 3. Potential energy surface for the reaction of R-triadimefon conformer A with two water molecules. Energies in black are relative energies compared to the separated reactants conformer A and water molecules; energies in red are relative energies compared to reactant complex $\mathbf{RC1}_{2W}$; and energies in blue are relative energies compared to reactant complex $\mathbf{RC2}_{2W}$. All energies are in kcal mol^{-1}

product complex 1 ($\mathbf{PC1}_{2w}$) is formed, which is 6.38 kcal mol^{-1} lower in energy than separated reactants but 11.50 kcal mol^{-1} higher than $\mathbf{RC1}_{2w}$. Similar to the one water reaction pathway, the enol forms after two water molecules leave $\mathbf{PC1}_{2w}$, then two waters tightly bond to the enol forming the reactant complex 2 ($\mathbf{RC2}_{2w}$, 14.89 kcal mol^{-1} (Table S5) lower in energy than separated enol and two waters). The final product complex 2 ($\mathbf{PC2}_{2w}$) again is favorably generated from $\mathbf{TS2}_{2w}$ since it is 17.88 kcal mol^{-1} lower in energy than conformer A plus two waters, 21.98 kcal mol^{-1} (Table S5) lower than enol plus two waters, and 7.09 kcal mol^{-1} lower than $\mathbf{RC2}_{2w}$.

Similar to the triadimefon plus one water reaction pathway, the reaction enthalpy, entropy, and Gibbs energy for reaction $\mathbf{RC1}_{2w} \rightarrow \mathbf{TS1}_{2w} \rightarrow \mathbf{PC1}_{2w}$ (Table S4) indicate that this part of the reaction is endothermic and would not occur spontaneously; the reaction $\mathbf{RC2}_{2w} \rightarrow \mathbf{TS2}_{2w} \rightarrow \mathbf{PC2}_{2w}$ is exothermic and spontaneous.

The optimized geometries of the six reactant complexes, transition states, and product complexes for the two water reaction pathway are listed in Table S6. Changes are similar to previous reaction pathway.

Conformer B Reaction With Hydroxide Ion

While both the one and two water pathways have higher reaction barriers than our experimental result (21.7 kcal mol^{-1}, average E_a of R-and S-triadimefon), and we have shown the reaction rates vary with pH, a reaction may take place between conformer B and hydroxide ion (Fig. 4). Differing from the previous one and two water molecule pathways, no large ring structure is formed when hydroxide is involved in the reaction. Instead, the oxygen from a hydroxide ion bonds to the most positively charged C_2 (+0.606 in Fig. S2) in reactant complex ($\mathbf{RC}_{OH}$, Fig. 4). The optimized geometries of reactant complexes, transition states, and product complexes for this pathway are shown in Table S7.

$\mathbf{RC}_{OH}$, $\mathbf{TS}_{OH}$, and $\mathbf{PC}_{OH}$ are 55.06, 36.80, and 62.57 kcal mol^{-1} lower in energy, respectively, than the separated triadimefon conformer B and hydroxide ion, and $\mathbf{PC}_{OH}$ is 7.52 kcal mol^{-1} lower than $\mathbf{RC}_{OH}$, indicating that this reaction is favorable. The local barrier for this pathway is 18.26 kcal mol^{-1}, which is much lower than the pathways involving water as the primary reactant and comparable to our experimental result (21.7 kcal mol^{-1}). Thus, it appears the hydroxide ion-based pathway is the most favorable for explaining triadimefon racemization.

The reaction enthalpy, entropy, and Gibbs energy for the reaction of triadimefon conformer B (TB) with hydroxide ion to form an enolate ion plus water (TB $+OH^- \rightarrow$enolate$^-+H_2O$) are shown in Table S8, which indicates that this part of the reaction is exothermic and will take place spontaneously even at low temperature.

The relative energies, enthalpies, entropies, and Gibbs energies of activation for all five transition states are summarized in Table 2. Different from $\mathbf{TS}_{OH}$, the Gibbs energy of activation for $\mathbf{TS1}_{1w}$, $\mathbf{TS2}_{1w}$, $\mathbf{TS1}_{2w}$, and $\mathbf{TS2}_{2w}$ are all positive; $\Delta G^{\ddagger}(\mathbf{TS1}_{2w})$ is 43.1 kcal mol^{-1}, the lowest among the four, which indicates that this reaction will take place very quickly. However, all four energies are much higher than the experimentally determined value 24.5 kcal mol^{-1} (average from R-and S-triadimefon). For the triadimefon + OH^- pathway, all these activation energies are negative, which

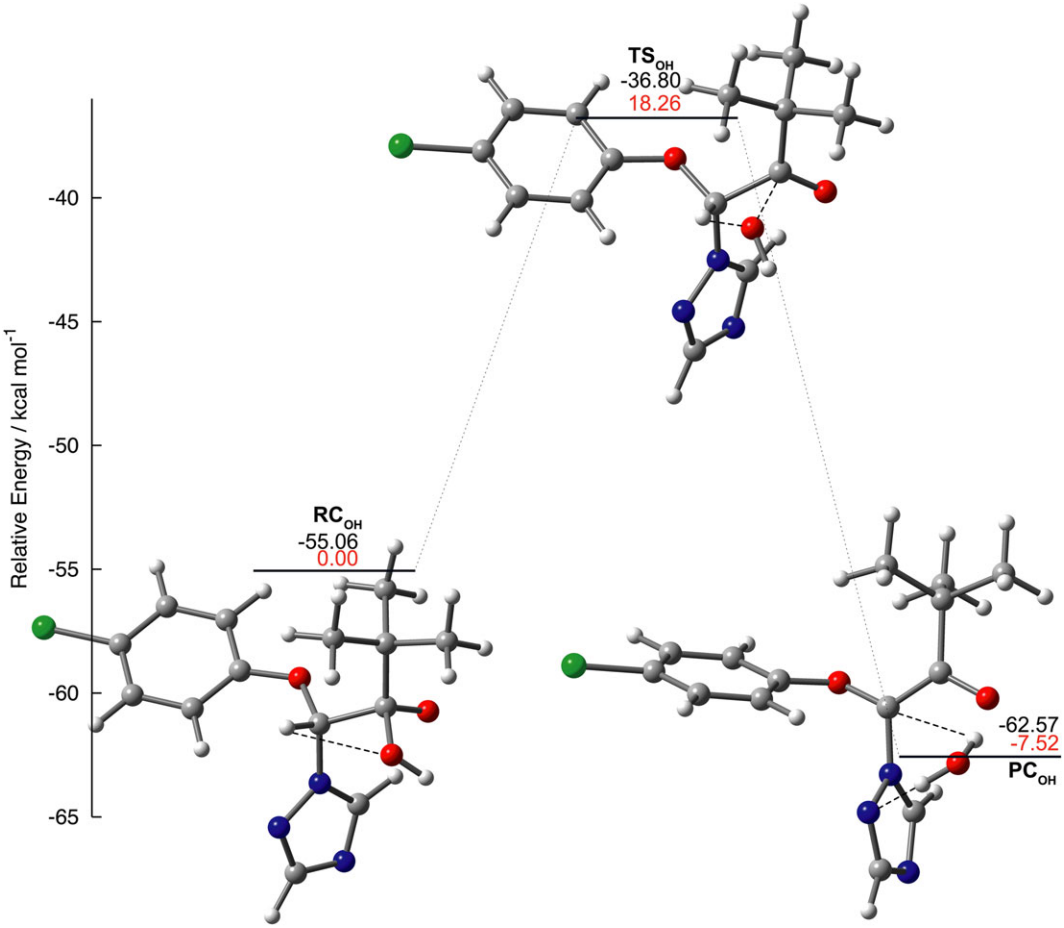

Fig. 4. Potential energy surface for the reaction path of conformer B plus hydroxide ion. Energies in black are relative energies compared to separated reactants conformer B and hydroxide ion, energies in red are the relative energies compared to (**RC**$_{OH}$). All energies are in kcal mol^{-1}

TABLE 2. Activation energy (ΔE, in kcal mol^{-1}), standard enthalpy of activation (ΔH‡, in kcal mol^{-1}), standard entropy of activation (ΔS‡, in cal mol^{-1} K^{-1}), and ordered Gibbs energies of activation (ΔG‡, in kcal mol^{-1}) with respect to separated reactants at 298.18 K

	ΔE kcal mol-1	ΔH‡ kcal mol-1	ΔS‡ kcal mol-1	ΔG‡ kcal mol-1
TS1$_{1w}$	36.55	33.18	−41.11	45.43
TS2$_{1w}$	40.84	37.68	−45.08	51.12
TS1$_{2w}$	23.11	19.93	−77.80	43.13
TS2$_{2w}$	24.80	22.30	−79.71	46.07
TS$_{OH}$	−36.80	−37.11	−36.61	−26.19

indicates that triadimefon racemization takes place easily and quickly. In this case the rate-determining step will be from the reactant complex to the transition state (after the reactant complex **RC**$_{OH}$, which lies 55.1 kcal mol^{-1} below separated B plus OH^{-}). The Gibbs energy is 15.3 kcal mol^{-1}, lower than experimental predicted value. These all indicate that the triadimefon reactions with water and OH^{-} may take place simultaneously. With increasing pH, the reaction favors the basic mechanism, so the reaction goes faster.

CONCLUSION

Enantiomers of chiral compounds can undergo interconversion leading to markedly different toxicities, which leads to uncertainty when evaluating potential risks to humans and the environment. Triadimefon is a chiral systemic 1,2,4-triazole fungicide; R-triadimefon is 2-fold more toxic than the racemate, and depending on the biological or environmental condition, triadimefon undergoes varying degrees of stereoselective reduction to yield triadimenol stereoisomers with differing toxicities. Because the degree of racemization can impact the distribution of triadimenol stereoisomers that are formed, we sought to better understand triadimefon racemization and enantiomerization reactions. We utilized both experimental and computational methods to determine the reaction site, rate-determining step, and most probable reaction pathways. Collectively, our results indicate that the reaction site is the alpha-carbonyl carbon and the rate-determining step is the cleavage of the C-H (C-D) bond. In addition, we have shown that the reaction is base-catalyzed and likely involves a symmetrical intermediate. This work provides an initial step in developing predictive, structure-based models for identifying chiral compounds of concern and should improve our understanding of the potential impact these compounds may have on human health and the environment.

ACKNOWLEDGMENTS

This research received funding from the U.S. Environmental Protection Agency (U.S. EPA) and by an appointment to the Postdoctoral Research Program at the Ecosystems Research Division, administered by the Oak Ridge Institute for Science

and Education through Interagency Agreement No. (DW8992298301) between the U.S. Department of Energy and the U.S. EPA. This research also used resources of the National Energy Research Scientific Computing Center, which is supported by the Office of Science of the U.S. Department of Energy under Contract No. DE-AC02-05CH11231. The views expressed in this article are those of the author[s] and do not necessarily represent the views or policies of the U.S. EPA. The authors declare they have no competing financial interests. We thank Professor Henry F. Schaefer, III, Dr. Jiande Gu, Dr. Keigo Ito, and Dr. Judy Wu for insightful discussions and technical expertise. Current address for Q. Cheng: School of Computational Sciences, Korea Institute for Advanced Study, 85 Hoegiro Dongdaemun-gu, Seoul, 02455, South Korea.

SUPPORTING INFORMATION

Additional supporting information may be found in the online version of this article at the publisher's web-site.

LITERATURE CITED

1. Boxall ABA, Rudd MA, Brooks BW, Caldwell DJ, Choi K, Hickmann S, Innes E, Ostapyk K, Staveley JP, Verslycke T, Ankley GT, Beazley KF, Belanger SE, Berninger JP, Carriquiriborde P, Coors A, Deleo PC, Dyer SD, Ericson JF, Gagné F, Giesy JP, Gouin T, Hallstrom L, Karlsson MV, Larsson DGJ, Lazorchak JM, Mastrocco F, McLaughlin A, McMaster ME, Meyerhoff RD, Moore R, Parrott JL, Snape JR, Murray-Smith R, Servos MR, Sibley PK, Straub JO, Szabo ND, Topp E, Tetreault GR, Trudeau VL, Van Der Kraak G. Pharmaceuticals and personal care products in the environment: what are the big questions? Environ Health Perspect 2012; 120: 1221–1229.
2. Garrison AW, Gan J, Liu W. Chiral pesticides: Stereo selectivity and its consequence. In: ACS Symposium Series 1085. American Chemical Society, 2012.
3. Rentsch KM. The importance of stereoselective determination of drugs in the clinical laboratory. J Biochem Biophys Methods 2002; 54: 1–9.
4. United States Environmental Protection Agency. EFED Interim Policy for Stereoisomeric Pesticides, Washington, DC. 2000. URL http://www2.epa.gov/pesticide-science-and-assessing-pesticide-risks/interim-policy-evaluation-stereoisomeric-pesticides.
5. European Union, Regulation (EC) No 1107/2009 of the European Parliament and of the Council of 21 October 2009 concerning the placing of plant protection products on the market and repealing Council Directives 79/117/EEC and 91/414/EEC, 2009. http://eurlex.europa.eu/LexUriServ/LexUriServ.do?uri=OJ:L:2009:309:0001:0050:EN:PDF.
6. Reist M, Testa B, Carrupt PA, Jung M, Schurig V. Racemization, enantiomerization, diastereomerization, and epimerization: Their meaning and pharmacological significance. Chirality 1995; 7: 396–400.
7. Ali I, Gupta VK, Aboul-Enein HY, Singh P, Sharma B. Role of racemization in optically active drugs development. Chirality 2007; 19: 453–463.
8. Li ZY, Zhang YC, Li QL, Wang WX, Li JY. Chiral separation and enantiomerization of triazole pesticides. Chin J Anal Chem 2010; 38: 237–240.
9. Kahle M, Buerge IJ, Hauser A, Muller MD, Poiger T. Azole fungicides: Occurrence and fate in wastewater and surface waters. Environ Sci Tech 2008; 42: 7193–7200.
10. Mantovani A, Maranghi F, La Rocca C, Tiboni GM, Clementi M. The role of toxicology to characterize biomarkers for agrochemicals with potential endocrine activities. Reprod Toxicol 2008; 26: 1–7.
11. Kellock K, Overmyer J, Garrison AW, Avants, JK. Toxicity of triadimefon racemate and enantiomers to black fly larvae. In: SETAC North America 30th Annual Meeting. New Orleans, LA, 2009, 296–297.
12. Kenneke JF, Mazur CS, Ritger SE, Sack TJ. Mechanistic investigation of the noncytochrome p450-mediated metabolism of triadimefon to triadimenol in hepatic microsomes. Chem Res Toxicol 2008; 21: 1997–2004.
13. Kenneke JF, Ekman DR, Mazur CS, Konwick BJ, Fisk AT, Avants JK, Garrison AW. Integration of metabolomics and in vitro metabolism assays for investigating the stereoselective transformation of triadimefon in rainbow trout. Chirality 2010; 22: 183–192.
14. Burden RS, Carter GA, Clark T, Cooke DT, Croker SJ, Deas AHB, Hedden P, James CS, Lenton JR. Comparative activity of the enantiomers of triadimenol and paclobutrazol as inhibitors of fungal growth and plant sterol and gibberellin biosynthesis. Pestic Sci 1987; 21: 253–267.
15. Yoshida Y, Aoyama Y. Stereoselective interaction of an azole antifungal agent with its target, lanosterol 14 α-demethylase (cytochrome p-450_{14DM}): a model study with steroeoisomers of triadimenol and purified cytochrome p-450_{14DM} from yeast. Chirality 1990; 2: 10–15.
16. Garrison AW, Avants JK, Jones WJ. Microbial transformation of triadimefon to triadimenol in soils: Selective production rates of triadimenol stereoisomers affect exposure and risk. Environ Sci Tech 2011; 45: 2186–2193.
17. Li Z, Zhang Y, Li Q, Wang W, Li J. Enantioselective degradation, abiotic racemization, and chiral transformation of triadimefon in soils. Environ Sci Tech 2011; 45: 2797–2803.
18. Reist M, Carrupt PA, Testa B, Lehmann S, Hansen JJ. Kinetics and mechanisms of racemization: 5-substituted hydantoins (= imidazolidine-2,4-diones) as models of chiral drugs. Helv Chim Acta 1996; 79: 767–778.
19. Nowell IW, Walker PE, Anderson NH. Structure of 1-(4-chlorophenoxy)-3,3-dimethyl-1-(1,2,4-triazol-1-yl)-2-butanone. Acta Crystallogr B 1982; 38: 1857–1859.
20. Chauhan J. Comparative x-ray structure analysis of systemic fungicides β-4(−chlorophenoxy)-α-(1,1 dimethylethyl) 1 h-1,2,4-triazole-1-ethanol and 1-(4-chlorophenoxy)3,3-dimethyl-1-h(1,2,4-triazole-1-y-1) 2-butanone. J Appl Sci Res 2008; 4: 166–170.
21. Chauhan J. Comparative X-ray crystallographic study on triazoles systemic fungicides. Int J Chem Tech Res 2009; 1: 208–211.
22. Carbonell E, Rothchild R. NMR studies of agricultural products. Applications of achiral and chiral lanthanide shift reagents to the fungicide, triadimefon. Spectrosc Lett 1994; 27: 861–878.
23. Becke AD. Density functional thermochemistry. III. The role of exact exchange. J Chem Phys 1993; 98: 5648–5652.
24. Lee C, Yang W, Parr RG. Development of the Colle-Salvetti correlation-energy formula into a functional of the electron density. Phys Rev B Condens Matter 1988; 37: 785–789.
25. Parr RG, Yang W. Density functional theory of atoms and molecules. Oxford University Press: New York; 1989.
26. Tirado-Rives J, Jorgensen WL. Performance of b3lyp density functional methods for a large set of organic molecules. J Chem Theory Comput 2008; 4: 297–306.
27. Duan XM, Song GL, Li ZH, Wang XJ, Chen GH, Fan KN. Accurate prediction of heat of formation by combining Hartree-Fock/density functional theory calculation with linear regression correction approach. J Chem Phys 2004; 121: 7086–7095.
28. Reed AE, Weinhold F. Natural bond orbital analysis of near Hartree–Fock water dimer. J Chem Phys 1983; 78: 4066–4073.
29. Reed AE, Weinhold F. Natural localized molecular orbitals. J Chem Phys 1985; 83: 1736–1740.
30. Reed AE, Weinstock RB, Weinhold F. Natural population analysis. J Chem Phys 1985; 83: 735–746.
31. Szabo A, Ostlund, NS. Modern quantum chemistry: introduction to advanced electronic structure theory. New York: Dover Publications; New edition, 1996.
32. Schaefer HF. Potential beneath the surface. Chem Britain 1975; 11: 227.
33. Fukui K. The path of chemical reactions - the IRC approach. Acc Chem Res 1981; 14: 363–368.
34. Schmidt MW, Gordon MS, Dupuis M. The intrinsic reaction coordinate and the rotational barrier in silaethylene. J Am Chem Soc 1985; 107: 2585–2589.
35. Garrett BC, Redmon MJ, Steckler R, Truhlar DG, Baldridge KK, Bartol D, Schmidt MW, Gordon MS. Algorithms and accuracy requirements for computing reaction paths by the method of steepest descent. J Phys Chem 1988; 92: 1476–1488.
36. Frisch MJ, Trucks GW, Schlegel HB, Scuseria GE, Robb MA, Cheeseman JR, Scalmani G, Barone V, Mennucci B, Petersson GA, Nakatsuji H, Caricato M, Li X, Hratchian HP, Izmaylov AF, Bloino J, Zheng G, Sonnenberg JL, Hada M, Ehara M, Toyota K, Fukuda R, Hasegawa J, Ishida M, Nakajima T, Honda Y, Kitao O, Nakai H, Vreven T, Montgomery Jr JA, Peralta JE, Ogliaro F, Bearpark M, Heyd JJ, Brothers E, Kudin KN, Staroverov VN, Kobayashi R, Normand J, Raghavachari K, Rendell A, Burant JC, Iyengar SS, Tomasi J, Cossi M, Rega N, Millam JM, Klene M, Knox JE, Cross JB, Bakken V, Adamo C, Jaramillo J, Gomperts R,

Stratmann RE, Yazyev O, Austin AJ, Cammi R, Pomelli C, Ochterski JW, Martin RL, Morokuma K, Zakrzewski VG, Voth GA, Salvador P, Dannenberg JJ, Dapprich S, Daniels A, Cioslowski J, Fox DJ. Gaussian 09 Revision A.1. Gaussian Inc: Wallingford, CT; 2009.

37. Carey FA, Sundberg RJ. Advanced organic chemistry part A: structure and mechanisms, 5th ed. Springer: New York; 2008.
38. Smith MB, March J. March's advanced organic chemistry: Reactions, mechanisms, and structure, 5th ed. John Wiley & Sons, Publication: New York; 2001.
39. Wilson CL. Prototropy in relation to the exchange of hydrogen isotopes. part II. A comparison of the velocities of dissociation of a proton and a deuteron from a Ψ-acid. J Chem Soc 1936; 1550–1553.